The Variance Risk Premium in Crude Oil Futures Markets: Incorporating the OVX Time Series in a Stochastic Volatility Model *

François Le Grand † Lorenz Schneider ‡

January 20, 2022

Abstract

In this paper we propose a stochastic volatility model for crude oil markets that has the particularity to feature a regime-switching price of variance-risk. While preserving tractability, this model allows us to capture the episodes of negative and positive variance risk premium. A two-state version of the model is estimated using the Kim (1994) filter on CBOE OVX volatility data. The model characterizes two states: a normal state with low volatility and negative variance premium and a crisis state with high volatility and positive variance risk premium. The estimated states are consistent with GDP data and anecdotal evidence. Incorporating regime information improves the performance of CAPM regressions.

Keywords: Variance Risk Premium· Stochastic Volatility · Regime-Switching · Oil Volatility Index (OVX) · Kim Filter

JEL: C63 · C52 · G13

*Many thanks to Lukas Harmuth, Alexander Langnau, Cassio Neri, Matthias Scherer and Bertrand Tavin for helpful and stimulating comments, discussions and suggestions. Part of this paper was written while the second author was KPMG Visiting Professor at the Technische Universität München.

†EMLYON Business School, legrand@em-lyon.com.

‡EMLYON Business School, schneider@em-lyon.com.

1 Introduction

Under normal circumstances, equity investors achieve a higher return on their capital than bondholders. In the classic Black and Scholes (1973) and Merton (1973) equity model, the actual $\mathbb{P}$-drift μ is higher than the risk-neutral $\mathbb{Q}$-drift r. Investors taking on risk expect to be rewarded. The equity risk-premium is positive. However, from time to time, there is a crisis, and the actual performance of shares falls below that of bonds.

The situation is reversed when it comes to realized $\mathbb{P}$-variances of share indices such as the S&P 500 and implied $\mathbb{Q}$-variances calculated from volatility indices such as the VIX. Under normal circumstances, the $\mathbb{P}$-variances are lower than the $\mathbb{Q}$-variances. The variance risk-premium is negative. One of the explanations for this phenomenon is that option sellers hedge the options they have sold, and during the hedging they are affected by the realized variance in the market. Clearly these option sellers expect to be rewarded, and they try to sell the options at a sufficiently high price, which in turn corresponds directly to the implied volatility. Again, however, a crisis occurs from time to time, and the situation turns around. For example, in October 2008, at the height of the financial crisis, the realized 21-day SPX variance reached a high of 0.6939, while the corresponding high of the squared VIX was lower at 0.6410. In March 2020, at the first shock of the Covid 19 crisis, the realized SPX variance reached 0.9064 and the squared VIX only 0.6838. Traders of variance swaps are familiar with this behaviour: usually, paying the $\mathbb{P}$-variance and receiving the $\mathbb{Q}$-variance is a profitable trade. However, in crisis periods, the trade can lead to significant losses. Here is how Alexander Langnau describes this trade (private communication):

> The presence of the volatility skew has as a consequence that the implied variance, which is deduced from options over a wide range of strikes, typically trades at a premium against the average variance. This behaviour motivated the creation of custom-tailored financial products where an investor would receive implied volatility on a monthly basis while paying realized volatility over the same period. Because of its excellent performance over back-testing periods, this product gained great popularity and traded in large size in the financial markets. It was only when the financial crisis hit in 2007 and investors lost up to 100% of their capital that the product showed its true down-side risk behaviour.

In this article, we focus on the variance risk premium (VRP) in crude oil markets. The introduction of the OVX, the crude oil volatility index, in 2007 has made such an endeavor much easier. In earlier studies in energy markets, such as Doran and Ronn (2008) and Trolle and Schwartz (2010), considerable effort was required to replicate such an index via liquid option quotes. Our starting point was the remark one often hears [1] that variance risk premia are notoriously difficult to estimate from financial time series. In most commodity models, the variance risk premium is represented by a single parameter. What if this parameter, instead of being constant over time, can undergo regime changes? And can these regime changes be detected by comparing time series of realized and implied variances?

Motivated by these questions, we allow the variance risk premium to switch between two states that are governed by an independent Markov chain. Intuitively, the first state corresponds to a "normal" regime with a negative VRP, and the second state to a "crisis" regime with a positive VRP. Of course, we do not *a priori* enforce these conditions, but let the data and estimation procedure lead us to our results.

At this point, we need to talk about the "historic" crisis of April 2020 that led to a negative WTI futures price for the first time in its history. On Monday, 20 April 2020, the then nearby May "K" contract closed at USD -37.63. (The following June "M" contract still closed with a positive price, as did the rest of the futures curve from there.) The previous closing price of the May contract, on Friday 17 April 2020, had been USD 18.27, implying a return of -306%. This crisis was so material that, when we include it in our estimation, it drastically changes the results. However, we believe that it would be premature to attach too much weight to this period. So far, it still remains a "unique" event, and it is difficult and unreliable to fit models to such singletons. In the same period, for example, the other crude oil benchmark, Brent, showed a more-or-less normal behaviour.

Therefore, we have decided to limit our study to OVX and realized-return data of CLc1 to the period from May 2007 to the beginning of March 2020. However, it is important to note that the events in April 2020 are completely in line with our narrative: The OVX peaked on 21 April 2020 at 325.15 points, or 3.2515 in absolute terms. Again, this was a historic high. But the realized volatility calculated for 21-day periods including

[1] for example by Eduardo Schwartz at the Commodity and Energy Markets Association (CEMA) Annual Meeting in Rome in June 2018

20 April 2020 lies above 11.6. And in terms of the variance: the corresponding squared OVX is 10.5723, in contrast with a realized variance above 130.

A Markov chain with M states has $M^2 - M$ transition probabilities that need to be specified or determined. It follows that increasing M leads to a large increase in the number of model parameters. Still, it could be interesting to add a third "really serious, historic" crisis or "pandemic" regime to our model and study the results. Currently, however, we believe that the data are too sparse to include such a third regime, and we also sincerely hope that things stay this way.

General introductions to the commodity finance literature are given in Clark (2014), Roncoroni et al. (2015), and Fanelli (2019). Doran and Ronn (2008) study the market price of volatility risk in energy markets using data from 1994 to 2004. Trolle and Schwartz (2009) study unspanned volatility in a stochastic volatility context, but don't focus on risk premia in particular. Trolle and Schwartz (2010) analyze variance risk premia in crude oil and natural gas markets using data from 1996 to 2006. Their approach is entirely model-free, in contrast to Doran and Ronn (2008) and our approach. Hamilton and Wu (2012) also study risk premia in crude oil markets, but focus on the futures price premium and not on the variance risk premium. Schneider and Tavin (2018) give the general multi-factor specification of the stochastic volatility model used here, and focus part of their attention on calibrating their model to volatility surfaces for crude oil futures and calendar spread options. Schneider and Tavin (2021) generalize the model to include seasonal volatility, give the state-space representation, and study time series of various agricultural commodities.

Regarding the filtering techniques we use in this article, our approach follow the contributions of Hamilton (1989), Lam (1990), and Kim (1994).

The remainder of this article is structured as follows. Section 2 presents our data and motivating evidence. Section 3 introduces the stochastic volatility model with a regime-switching variance-risk parameter. In Section 4, we present our empirical results. In particular, we compare the performance of the static 1-state model to the regime-switching 2-state model. We also examine the probabilities we obtain for being in the "crisis" state at certain times and investigate whether they correspond to real-world events. Furthermore, we examine whether the performance of a Capital Asset Pricing Model (CAPM) can be improved by including information about the current regime. Section 6 concludes the article.

2 Data and motivating evidence

In this section, we present the set of data we are using, as well as some motivating evidence for the model we develop. Our analysis uses two main sources of data related to the oil market: the Crude Oil Volatility Index (OVX), and the NYMEX WTI Crude Oil futures prices.

The OVX is a volatility index for crude oil markets. This index is similar to the well-known Volatility Index (VIX) for the S&P500 stock index. According to the CBOE, "the Cboe Crude Oil ETF Volatility Index measures the market's expectation of 30-day volatility of crude oil prices by applying the VIX methodology to United States Oil Fund, LP (Ticker - USO) options spanning a wide range of strike prices." We take this index as a measure of *implied volatility* and its square as a measure of *implied variance*.

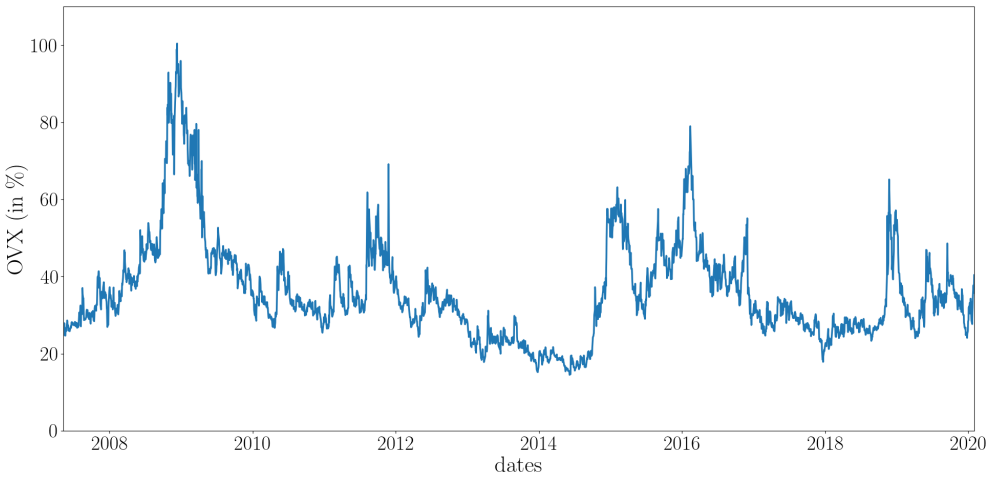

Figure 1: The OVX from 10 May 2007 to 31 January 2020.

Even though the OVX has been published since 15 July 2008, daily OVX data are available going further back to 10 May 2007 from the CBOE, we choose this earlier date as the natural starting point of our empirical analysis. Figure 1 plots the evolution of OVX from 10 May 2007 to 31 January 2020. [2] Our whole analysis in the remainder of this paper will be based on this time window. The OVX (resp. OVX^2) peaked at 100.42%

[2]The OVX is expressed in *points*, where 100 corresponds to an implied volatility level of 100%, but for mathematical convenience, we will consider it as expressed in *percentage points*, where 1 corresponds to an implied volatility level of 100%.

(100.84%) on 11 December 2008, and reached its lowest point of 14.50% (2.10%) on 6 June 2014. We report in Table 1 some basic descriptive statistics regarding OVX.

	OVX	OVX^2
Mean	36.02%	14.70%
Standard Error	13.13%	12.47%
Minimum	14.50%	2.10%
	(on 6 June 2014)	
Q25	27.72%	7.68%
Median	33.19%	11.02%
Q75	41.97%	17.61%
Maximum	100.42	100.84%
	(on 11 December 2008)	

Table 1: Descriptive statistics on OVX and OVX^2 (between 10 May 2007 and 31 January 2020).

Regarding futures prices, we consider the NYMEX WTI Crude Oil futures data (henceforth, CL) from Thomson Reuters. The data consist of the running futures series of 24 futures contracts. For instance, CLc1 denotes the futures contract that arrives to maturity within the next month. This is the earliest available maturity. Oppositely, CLc24 is the futures contract with the latest available maturity, that lies between 23 and 24 months from the date under consideration. These series are constructed by concatenating the first futures price with the new first futures price after the roll date, and so on. In contrast to other commodity markets, such as agriculturals or electricity, there is no seasonality in crude oil markets. We plot in Figure 2 the time evolution of CLc1 and CLc24 from 10 May 2007 to 2 March 2020. As can be seen, both price time-series are highly correlated – the correlation coefficient amounting to 93.04%. The shorter contract CLc1 is however more volatile than the longer one CLc24, which is a manifestation of the Samuelson volatility effect (see Schneider and Tavin, 2018, for instance). This effect is the empirical observation from most commodity markets that a given contract increases in volatility as it approaches its maturity date.

Table 2 gathers some basic statistics regarding CLc1 and CLc24. In particular, the Samuelson effect is visible in the standard error of the CLc24 that is lower than the one

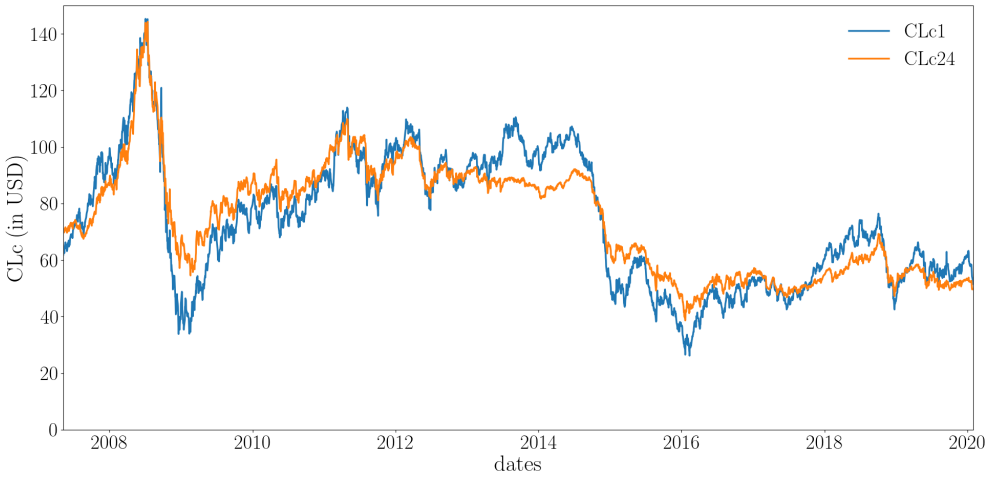

Figure 2: The CLc1 and CLc24 from 10 May 2007 and 31 January 2020.

of CLc1.

	CLc1	CLc24
Mean	74.07	74.59
Standard Error	22.99	19.59
Minimum	26.21 (on 11 Feb 2016)	38.66 (on 20 Jan 2016)
Q25	53.27	55.06
Median	72.47	77.54
Q75	93.82	88.81
Maximum	145.29 (on 3 Jul 2008)	144.26 (on 14 Jul 2008)

Table 2: Descriptive statistics on CLc1, and CLc24 (values in USD), from 10 May 2007 to 31 January 2020.

As we wish to compare the implied variance from the OVX with the realized variance of the CLc1 futures contract, we need to calculate 30-day realized variances. We denote by $F(t, T_1)$ the price at date t of the futures contract CLc1 maturing at date T_1. We consider a time period of N business days corresponding to the set of trading dates $t_0 < t_1 < \ldots < t_N$, with $\Delta t = t_i - t_{i-1} = 1/252$. In our computations, we will solely

focus on $N = 21$ trading days. The realized variance of the futures contract over these N dates will be denoted by $\mathrm{RV}^{\mathrm{CLc1}}_{t_0,t_N}$ for the sake of simplicity, as N remains unchanged in the remainder of the paper. This realized variance can be computed as follows:

$$\mathrm{RV}^{\mathrm{CLc1}}_{t_0,t_N} = \frac{1}{\triangle t}\frac{1}{N-1}\sum_{i=1}^{N}\left(\ln\frac{F(t_i,T_1)}{F(t_{i-1},T_1)} - \mu_{t_0,t_N}\right)^2,$$

where μ_{t_0,t_N} is the N-day sample mean (similarly denoted without N) computed as:

$$\mu_{t_0,t_N} = \frac{1}{N}\sum_{i=1}^{N}\ln\frac{F(t_i,T_1)}{F(t_{i-1},T_1)}.$$

Note that the quantities $\mathrm{RV}^{\mathrm{CLc1}}_{t_0,t_N}$ and μ_{t_0,t_N} are only known at date t_N, which explains why we use two time subscripts for these quantities. The realized volatility can simply be computed as the square root of the realized variance. We report in Table 3 descriptive statistics regarding the one-month realized variance of the futures contact CLc1 and the implied variance, OVX^2.

We will report two versions for the realized variance. In the first one, we will report the realized variance that covers the same time span as the implied variance of the same date. More precisely, since at a given date t, we will report the implied variance OVX^2_t that spans the time period from date t to date $t+20$, the associated realized variance will be the one that covers the same time interval, which is $\mathrm{RV}^{\mathrm{CLc1}}_{t,t+20}$. The second version of the realized variance will be based on the information available at a given date. At any date t, the known implied variance is still OVX^2_t, while the known realized variance is $\mathrm{RV}^{\mathrm{CLc1}}_{t-20,t}$. This explains the small difference in the column OVX^2 compared to Table 1, as well as the fact that the sample goes from 10 May 2007 to 31 January 2020 (which is exactly 21 days before 2 March 2020).

We plot in Figure 3 the OVX^2 together with the two CLc1 realized variance time series. For clarity purposes, we split the figures into two panels. The top panel corresponds to $\mathrm{RV}^{\mathrm{CLc1}}_{t,t+20}$, where the realized variance spans the same time period as the implied variance OVX^2_t, while the bottom panel reports $\mathrm{RV}^{\mathrm{CLc1}}_{t-20,t}$, which is known at the same time as the implied variance OVX^2_t. Obviously, both panels display similar graphs, even though the spikes in the $\mathrm{RV}^{\mathrm{CLc1}}_{t-20,t}$ graph seem to be more aligned than in the OVX^2_t. This better coincidence is also visible in the larger correlation with realized variance of

	Implied variance (OVX_t^2)	Realized variance ($\text{RV}_{t,t+20}^{\text{CLc1}}$)	Realized variance ($\text{RV}_{t-20,t}^{\text{CLc1}}$)
Mean	14.70%	13.64%	13.64%
Standard Error	12.47%	18.28%	18.28%
Minimum	2.10% (on 6 Jun 2014)	0.96% (on 3rd Jan 2013)	0.96% (on 1st Feb 2013)
Q25	7.68%	4.70%	4.70%
Median	11.02%	7.68%	7.68%
Q75	17.61%	14.40%	14.40%
Maximum	100.84% (on 11 Dec 2008)	151.50% (on 8 Dec 2008)	151.50% (on 7 Jan 2009)
Correlation with OVX_t^2	100.0%	83.0%	86.4%

Table 3: Realized vs Implied variance, from 10 May 2007 to 31 January 2020.

$\text{RV}_{t-20,t}^{\text{CLc1}}$ compared to $\text{RV}_{t,t+20}^{\text{CLc1}}$. This shows that realized variance somehow drives implied variance.

We have reported variances rather than volatilities in Table 3 and Figure 3, even though considering the latter would have produced very similar outcomes. The reason we opted for variances is that traded derivatives, such as variance swaps for instance, are based on variances rather than volatilities. Following the literature (see Carr and Wu, 2009 and Trolle and Schwartz, 2010 among others), we define the variance risk premium as the difference between the realized variance at date t and the implied variance 21 days before:

$$\text{VRP}_{t,t+20} = \text{RV}_{t,t+20}^{\text{CLc1}} - \text{OVX}_t^2. \tag{1}$$

The variance risk premium can be seen as the payoff of a swap contract in which the buyer of the contract pays the fixed leg OVX_t^2 and receives the floating leg, equal to $\text{RV}_{t,t+20}^{\text{CLc1}}$, 21 days later. As such the variance risk premium is only known at date $t+20$. Similarly, the variance risk premium in log return terms is defined as follows:

$$\text{VRPL}_{t,t+20} = \ln(\text{RV}_{t,t+20}^{\text{CLc1}}/\text{OVX}_t^2). \tag{2}$$

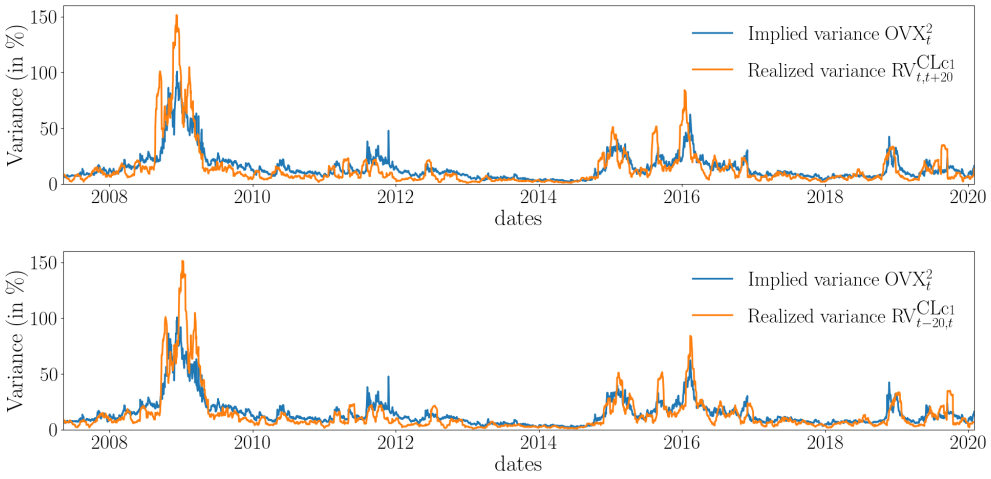

Figure 3: OVX^2 and CLc1 realized variance, from 10 May 2007 to 31 January 2020.

Because of these trading contracts, the focus of the present paper will be mostly on the implied variance series $(OVX_t^2)_t$. We will denote it as OVX2 and there should not be any ambiguity on the fact that we refer to the lagged time-series that is consistent with the variance risk premium, and not to time-series that is consistent with the time-t available information.

As can be observed in the top panel of Figure 3, the OVX2 series lies above the CLc1 series most of the time. This is reflected in a variance risk premium (VRP, henceforth) that is negative most of of the time and on average. However, the sample also features periods, in which the CLc1 surpasses the OVX2, implying a positive VRP. These periods seem to correspond to periods with very high realized volatilities. So as to better contrast the episodes of positive and negative variance risk premium, we report several conditional statistics in Table 5. The first column, labeled "Unconditional", reports unconditional means and unconditional standard errors for the whole sample. The second column, labeled "Positive VRP" reports means and standard errors conditional on episodes of positive VRP. For instance, the "positive VRP" conditional mean of a generic variable x is defined as:

$$\overline{x}^{\text{VRP}>0} = \frac{\sum_{t=0}^{T} x_t 1_{\text{VRP}_{t-20,t}>0}}{\sum_{t=0}^{T} 1_{\text{VRP}_{t-20,t}>0}}, \tag{3}$$

where T is the size of our sample and $1_{\text{VRP}_{t-20,t}>0}$ an indicator function equal to 1 if $\text{VRP}_{t-20,t} > 0$ and 0 otherwise. The standard error is defined in a very similar way.

Finally, the last column in Table 5, labeled "Negative VRP", reports means and standard errors conditional on the VRP being negative. The formal definition parallels the one of equation (3).

	Unconditional	Positive VRP	Negative VRP
Number of observations	3185	842	2343
$\mathrm{VRP}_{t-20,t}$ (%)	-1.04 (10.58)	9.93 (14.60)	-4.98 (4.10)
Realized variance $\mathrm{RV}^{\mathrm{CLc1}}_{t,t+20}$ (%)	13.68 (18.33)	21.31 (25.18)	10.94 (14.17)
Realized variance $\mathrm{RV}^{\mathrm{CLc1}}_{t-20,t}$ (%)	13.68 (18.33)	28.42 (28.55)	8.38 (7.61)
OVX2 (%) (OVX^2_t)	14.75 (12.49)	22.55 (18.16)	11.94 (8.00)
CLc1 price $F(t, T_1)$ (USD)	74.13 (23.04)	67.76 (23.77)	76.41 (22.34)
1-day CLc1 log-return (%)	-0.01 (2.38)	-0.01 (3.46)	-0.01 (1.85)
21-day CLc2 log-return (%)	-0.86 (10.02)	-5.02 (12.55)	0.63 (8.47)

Table 4: Conditional statistics regarding episodes of positive and negative VRP.

Table 5 makes it clear that the behavior of time-series is very different during episodes of positive VRP compared to episodes of negative VRP, while unconditional means tend to minimize the contrast between the two. The differences among the two episodes obviously concern the VRP, but also realized variance, OVX2, and to a lesser extent CLc1 prices and returns. In short, positive VRP episodes feature high realized variance (and hence high volatility), high values of the OVX2, but low prices. One-day returns are not significantly affected, while 21-day returns are negative when VRP is positive. Oppositely, negative VRP episodes are characterized by low (or moderate) realized variance, low values of the OVX2, and moderate or high prices, as well as (barely) positive 21-day returns. We can also observe that the overall volatility (reflected in the standard of the different quantities

reported Table 5) tends to be higher in periods of positive VRP than in period of negative ones.

These elements let us think that episodes of positive or negative VRP are of different nature and correspond to different regimes in the oil market. This is consistent with the anecdotal evidence of Figure 3. The positive VRP episodes correspond to well-known episodes: the 2008 crisis, the 2011 European economic crisis, the European debt crisis in 2012, the conjunction of Middle-East (especially in Libya) and Ukraine problems in 2015, the 11-year low of the WTI price implying production uncertainties in 2016. This means that positive VRP episodes can be connected to particular events of the last 15 years – that we will call crisis. This denomination of crisis is obviously a simplification since it covers episodes of very different magnitudes, some of them having a strong and international span that affects a vast majority financial markets (e.g., 2008 crisis), some of them being more local (European crisis) or more specific to the oil market (11-year low of the WTI price).

3 A Regime-Switching Stochastic Volatility Model for Crude Oil Futures

3.1 Our modeling choices

We now explain how the empirical evidence of Section 2 has led us shape our model and in particular to opt for a regime-switching model. Before turning to the technical details, we will walk through the main steps of the model in a non-technical way. Our model can be seen as being made of three distinct layers. The first layer builds on the Clewlow and Strickland (1999) model, which is one of the seminal models for the valuation of commodity derivatives. The model is futures-based. It assumes that, under the risk-neutral probability, the instantaneous return of the futures follows a uni-dimensional normal distribution. The expectation of this distribution is null because futures contracts do not require any initial investment. The volatility is a negative exponential function that guarantees the spot price to be Markovian. From an empirical perspective, this allows the model to incorporate the Samuelson (1965) volatility effect. The second layer involves introducing stochastic volatility à la Heston (1993). The combination of these

two ingredients yields the model given in Schneider and Tavin (2018). The third layer concerns the risk premium, and hence the change of measure from the risk-neutral to the physical probability. Instead of considering a constant market price of risk, we assume that the price of risk is regime-switching. The objective of this choice is to account for the episodes of negative and positive VRP that we discussed in Section 2. However, it remains a quantitative question whether the price of risk will actually be estimated with different signs.

One of the strengths of our model is its relatively good tractability. Introducing regime-switching in stochastic models in general leads to tractability issues. For instance, Elliott et al. (2005) explain that, because of market-incompleteness, the martingale measure is not unique and they opt for the so-called minimal entropy martingale measure. Papanicolaou and Sircar (2014) make their VIX options pricing model tractable by considering a Taylor development of the model around small rates of regime switches. However, our model preserves tractability, as the specification under the risk-neutral measure $\mathbb{Q}$ is unchanged, while still allowing for regime-switches that only affect the model dynamics under the physical measure $\mathbb{P}$. Our model therefore enables us to combine tractability with regime-switching that can be estimated using the Kim (1994) filter, which is an adaptation of the Kalman filter to regime-switching models.

The rest of the section is organized as follows: In Section 3.2, we present the model, while in Section 3.3, we provide the model's state-space representation that allows us to estimate it using the Kim filter.

3.2 The model

Under the risk-neutral probability measure $\mathbb{Q}$. We begin by giving a mathematical description of our model under the risk-neutral measure $\mathbb{Q}$. Let $B_1^{\mathbb{Q}}, B_2^{\mathbb{Q}}$ be Brownian motions under $\mathbb{Q}$. Let T_m be the maturity of a given futures contract CLm. The futures price $F(t, T_m)$ at time $t, 0 \leq t \leq T_m$, is assumed to follow the stochastic differential equation (SDE)

$$dF(t, T_m) = F(t, T_m)e^{-\lambda(T_m - t)}\sqrt{v_t}dB_{1,t}^{\mathbb{Q}} \tag{4}$$

and the variance process (v_t) to follow the SDE

$$dv_t = \kappa\left(\theta - v_t\right)dt + \sigma\sqrt{v_t}dB_{2,t}^{\mathbb{Q}}. \tag{5}$$

The correlation is given by $\langle dB^{\mathbb{Q}}_{1,t}, dB^{\mathbb{Q}}_{2,t}\rangle = \rho dt$.

It is well-known that v_T follows a noncentral chi-squared distribution (see Cox et al. (1985)). At current time $t = 0$ and for a given time-horizon T, the density of v_T can be written in terms of the modified Bessel function of the first kind I_q as

$$g(v_T; T, v_0) = ce^{-u-w}\left(\frac{w}{u}\right)^{q/2} I_q(2\sqrt{uw}), \tag{6}$$

where v_0 is the initial variance value and

$$c := \frac{2\kappa}{\sigma^2(1-e^{-\kappa T})},\ u := cv_0e^{-\kappa T},\ w := cv_T,\ q := \frac{2\kappa\theta}{\sigma^2} - 1.$$

European call and put options on futures contracts can be priced using the Fourier inversion technique as described in Heston (1993) and Bakshi and Madan (2000). The characteristic function of the model is given in Schneider and Tavin (2018). There it is also shown that the model performs well when calibrated to futures and option prices, since it can perfectly match any given futures curve and provide a good fit for the option implied volatility strike- and term-structure, and that it outperforms both the 1-factor Clewlow and Strickland (1999) model and the Heston (1993) model.

Under the physical probability measure $\mathbb{P}$. To specify the model under the physical probability measure $\mathbb{P}$, we follow the "completely affine" specification of Casassus and Collin-Dufresne (2005) (see also Doran and Ronn (2008), Trolle and Schwartz (2009), and Chiarella et al. (2013)). We use the relations

$$dB^{\mathbb{P}}_{1,t} = dB^{\mathbb{Q}}_{1,t} - \pi^F\sqrt{v_t}dt, \tag{7}$$
$$dB^{\mathbb{P}}_{2,t} = dB^{\mathbb{Q}}_{2,t} - \pi^v\sqrt{v_t}dt, \tag{8}$$

where the parameter π^F gives the *market price of futures risk*, and the parameter π^v the *market price of variance risk*.

It ensues that for fixed T_m, the futures price $F(t, T_m)$ under $\mathbb{P}$ follows the SDE

$$\begin{aligned} dF(t,T_m) &= F(t,T_m)e^{-\lambda(T_m-t)}\sqrt{v_t}dB^{\mathbb{Q}}_{1,t} \\ &= F(t,T_m)\left(\pi^F e^{-\lambda(T_m-t)}v_t dt + e^{-\lambda(T_m-t)}\sqrt{v_t}dB^{\mathbb{P}}_{1,t}\right), \end{aligned} \tag{9}$$

and the variance process v follows the SDE

$$\begin{aligned} dv_t &= \kappa\left(\theta - v_t\right) dt + \sigma\sqrt{v_t} dB_{2,t}^{\mathbb{Q}}, \\ &= \left(\kappa\left(\theta - v_t\right) + \sigma\pi^v v_t\right) dt + \sigma\sqrt{v_t} dB_{2,t}^{\mathbb{P}}. \end{aligned} \tag{10}$$

Introducing new parameters

$$\tilde{\kappa} := \kappa - \sigma\pi^v, \quad \tilde{\theta} := \frac{\kappa\theta}{\kappa - \sigma\pi^v} = \frac{\kappa}{\tilde{\kappa}}\theta, \tag{11}$$

this process can be written in the familiar form as

$$dv_t = \tilde{\kappa}\left(\tilde{\theta} - v_t\right) dt + \sigma\sqrt{v_t} dB_{2,t}^{\mathbb{P}}.$$

The futures premium π^F introduces a drift term into the SDE (9) for the futures returns, which is proportional to π^F and damped by the exponential factor. It has no effect on the volatility. If $\pi^F > 0$, futures prices will have a tendency to rise, and if $\pi^F < 0$, futures prices will have a tendency to fall.

The variance premium π^v only affects the drift term of the SDE (10) for the variance. If $\pi^v > 0$, the mean-reversion rate $\tilde{\kappa}$ will be reduced and the mean-reversion level $\tilde{\theta}$ will be increased, and if $\pi^v < 0$, $\tilde{\kappa}$ will be increased and $\tilde{\theta}$ will be reduced.

3.3 Model estimation using the Kim filter

The state-space representation of the model. A general Gaussian linear state-space model with regime-switching is given by a *transition equation*

$$\boldsymbol{s}_t = \boldsymbol{d}_t^{S_t} + \boldsymbol{T}_t^{S_t}\boldsymbol{s}_{t-1} + \boldsymbol{R}_t^{S_t}\boldsymbol{\eta}_t^{S_t}, \tag{12}$$

and a *measurement equation*

$$\boldsymbol{y}_t = \boldsymbol{c}_t^{S_t} + \boldsymbol{Z}_t^{S_t}\boldsymbol{s}_t + \boldsymbol{e}_t^{S_t}, \tag{13}$$

for time $t \in \{1, \ldots, T\}$, with state $\boldsymbol{s}_t \in \mathbb{R}^{q\times 1}$, $\boldsymbol{d}_t^{S_t} \in \mathbb{R}^{q\times 1}$, $\boldsymbol{T}_t^{S_t} \in \mathbb{R}^{q\times q}$, $\boldsymbol{R}_t^{S_t} \in \mathbb{R}^{q\times r}$, $\boldsymbol{\eta}_t^{S_t} \sim \mathcal{N}_r(0, \boldsymbol{Q}_t^{S_t})$, $\boldsymbol{Q}_t^{S_t} \in \mathbb{R}^{r\times r}$ denoting the system vectors and matrices of the transition equation, and measurement $\boldsymbol{y}_t \in \mathbb{R}^{p\times 1}$, $\boldsymbol{c}_t^{S_t} \in \mathbb{R}^{p\times 1}$, $\boldsymbol{Z}_t^{S_t} \in \mathbb{R}^{p\times q}$, $\boldsymbol{e}_t^{S_t} \sim \mathcal{N}_p\left(0, \boldsymbol{H}_t^{S_t}\right)$,

$\boldsymbol{H}_t^{S_t} \in \mathbb{R}^{p\times p}$ denoting the system vectors and matrices of the measurement equation. We follow here the notation of a state-model as given in Tsay (2010).

The superscript S_t implies that the parameters of the system vectors and matrices depend on a hidden Markov chain. More precisely, we model S_t as the outcome of an unobserved discrete-time, discrete-state Markov process with M different regimes. We interpret the outcomes of S_t as states or regimes, i.e., $S_t = i$ means that the process is in regime i at time t. The transition probability

$$p_{i,j} := \mathrm{P}\left(S_t = j | S_{t-1} = i\right) \tag{14}$$

is defined as the probability of switching from regime i to regime j.

We now proceed to extend the Schneider and Tavin (2018) model to incorporate a regime-switching variance risk premium, the third layer in our "modelling choices" described above. The parameter π^v is assumed to depend on a hidden Markov chain S_t, that is, we consider a set of parameters π^{v,S_t} from now on. Concretely, we assume $S_t \in \{0, 1\}$ in the following as a 2-state Markov chain, where the state $S_t = 0$ represents the "normal" state and the state $S_t = 1$ a "crisis" state in the model. The transition probabilities are given by

$$P = \begin{pmatrix} p_{0,0} & p_{0,1} \\ p_{1,0} & p_{1,1} \end{pmatrix}, \tag{15}$$

with $\sum_{j=0}^{1} p_{i,j} = 1$ for $i = 0, 1$. Led by our initial empirical inspection of our data, we conjecture that the variance risk premium - and therefore also the risk premium parameter π^v - is negative in times of "normal" low market variances ($S_t = 0$) and positive in times of "crisis" market turmoil ($S_t = 1$). The aim is then to apply the Kim filter to calculate the probabilities of the model being in this crisis state $S_t = 1$.

To carry out this investigation, we will compare 21-day realized variance from the CLc1 futures contract to the implied variance given by the square of the OVX to determine the variance risk premium. We make two assumptions at this stage. First, since we are studying the nearby CLc1 series which is very close to maturity, we set the Samuelson damping parameter λ of the full model to zero when calculating the realized 21-day variance. Another reason for our choice of $\lambda = 0$ is that we are only working with

the CLc1 series, but not any other contracts along the futures curve; since we don't see any term-structure of variances, we believe that the parameter λ cannot be estimated accurately in any case. Second, we assume that the realized variance $\mathrm{RV}_t^{\mathrm{CLc1}}$ is represented by the integrated expected variance under the physical measure $\mathbb{P}$. So with a slight abuse of notation, we denote the random variable and its estimator by the same variable. From the specification of the Schneider and Tavin (2018) model, we can work out that

$$\mathrm{RV}_t^{\mathrm{CLc1}} = \frac{1}{T-t}\int_t^T \mathbb{E}^{\mathbb{P}}[v_s|\mathcal{F}_t]ds = \tilde{\theta}\left(1 - \frac{1-e^{-\tilde{\kappa}\tau}}{\tilde{\kappa}\tau}\right) + \frac{1-e^{-\tilde{\kappa}\tau}}{\tilde{\kappa}\tau}v_t, \tag{16}$$

$$\mathrm{OVX}_t^2 = \frac{1}{T-t}\int_t^T \mathbb{E}^{\mathbb{Q}}[v_s|\mathcal{F}_t]ds = \theta\left(1 - \frac{1-e^{-\kappa\tau}}{\kappa\tau}\right) + \frac{1-e^{-\kappa\tau}}{\kappa\tau}v_t. \tag{17}$$

Comparing equations (16) and (17), we obtain the following expression of the variance risk premium in our model:

$$\begin{aligned}\mathrm{VRP}_t &= \mathrm{RV}_t^{\mathrm{CLc1}} - \mathrm{OVX}_t^2 \\ &= \tilde{\theta}\left(1 - \frac{1-e^{-\tilde{\kappa}\tau}}{\tilde{\kappa}\tau}\right) - \theta\left(1 - \frac{1-e^{-\kappa\tau}}{\kappa\tau}\right) + \left(\frac{1-e^{-\tilde{\kappa}\tau}}{\tilde{\kappa}\tau} - \frac{1-e^{-\kappa\tau}}{\kappa\tau}\right)v_t.\end{aligned} \tag{18}$$

To show that the sign of the parameter π^{v,S_t} corresponds to the sign of the VRP, we approximate the exponential terms appearing in (18) with a second-order Taylor polynomial around zero and find

$$\begin{aligned}\mathrm{VRP}_t &\doteq \tilde{\theta}\left(1 - \frac{1-\left(1-\tilde{\kappa}\tau+\frac{1}{2}(\tilde{\kappa}\tau)^2\right)}{\tilde{\kappa}\tau}\right) - \theta\left(1 - \frac{1-\left(1-\kappa\tau+\frac{1}{2}(\kappa\tau)^2\right)}{\kappa\tau}\right) \\ &\quad + \left(\frac{1-\left(1-\tilde{\kappa}\tau+\frac{1}{2}(\tilde{\kappa}\tau)^2\right)}{\tilde{\kappa}\tau} - \frac{1-\left(1-\kappa\tau+\frac{1}{2}(\kappa\tau)^2\right)}{\kappa\tau}\right)v_t \\ &= \tilde{\theta}\left(1-(1-\frac{1}{2}\tilde{\kappa}\tau)\right) - \theta\left(1-(1-\frac{1}{2}\kappa\tau)\right) + \left(1-\frac{1}{2}\tilde{\kappa}\tau-(1-\frac{1}{2}\kappa\tau)\right)v_t \\ &= \frac{1}{2}\tilde{\kappa}\tau\tilde{\theta} - \frac{1}{2}\kappa\tau\theta + \frac{1}{2}\left(\kappa-\tilde{\kappa}\right)\tau v_t \\ &= \frac{1}{2}\tilde{\kappa}\tau\frac{\kappa}{\tilde{\kappa}}\theta - \frac{1}{2}\kappa\tau\theta + \frac{1}{2}\left(\kappa-(\kappa-\sigma\pi^v)\right)\tau v_t \\ &= \frac{1}{2}\sigma\pi^v\tau v_t.\end{aligned} \tag{19}$$

Clearly, the expression (19) is positive if π^v is positive, and negative if π^v is negative, since σ and $v(t)$ are both (strictly) positive. Therefore, the two signs do indeed coincide.

A "simple" model for the variance risk premium. It is clear from these expressions that our study of the VRP in fact only depends on the variance processes (5) and (10) under the probability measures $\mathbb{Q}$ and $\mathbb{P}$, respectively, but not on the futures SDEs (4) and (9). From now on, we therefore focus our attention to the nested "simple" model for the variance given by equations (5), (10), and the change-of-measure equation (8).

We take the instantaneous variance v_t from the Schneider and Tavin (2018) one-factor model as state vector $\boldsymbol{s}_t$ and set the transition equation as

$$\begin{aligned}\boldsymbol{s}_t = (v_t) &= \boldsymbol{d}_t + \boldsymbol{T}_t^{S_t}\boldsymbol{s}_{t-1} + \boldsymbol{R}_t^{S_t}\boldsymbol{\eta}_t \\ &= \left(\kappa\theta\Delta t\right) + \left(1 - \left(\kappa - \sigma\pi^{v,S_t}\right)\Delta t\right)\boldsymbol{s}_{t-1} + \left(\sigma\sqrt{\boldsymbol{s}_{t-1}^{S_t}}\right)\boldsymbol{\eta}_t, \end{aligned} \tag{20}$$

where

$$\boldsymbol{\eta}_t \sim \mathcal{N}\left(0, \boldsymbol{Q}_t\right), \tag{21}$$

and with initial condition

$$\boldsymbol{s}_0 = (v_0) \in \mathbb{R}^{1\times 1}. \tag{22}$$

Concretely, we set

$$\boldsymbol{d}_t = \left(\kappa\theta\Delta t\right) \in \mathbb{R}^{1\times 1}, \tag{23}$$

the transition matrix

$$\boldsymbol{T}_t^{S_t} = \left(1 - \left(\kappa - \sigma\pi^{v,S_t}\right)\Delta t\right) \in \mathbb{R}^{1\times 1}, \tag{24}$$

$$\boldsymbol{R}_t^{S_t} = \left(\sigma\sqrt{\boldsymbol{s}_{t-1}^{S_t}}\right) \in \mathbb{R}^{1\times 1}, \tag{25}$$

and

$$\boldsymbol{Q}_t = \Big(\Delta t\Big) \in \mathbb{R}^{1\times 1}. \tag{26}$$

Now, the parameter π^{v,S_t} depends on the state of the Markov chain S_t, and it follows that the matrices $\boldsymbol{T}_t^{S_t}$ and $\boldsymbol{R}_t^{S_t}$ also become state-dependent.

Although the transition equation (15) is one-dimensional, we continue using bold letters, indicating vectors and matrices, and interpret $\boldsymbol{s}_t$, $\boldsymbol{d}_t$, $\boldsymbol{\eta}_t$, and $\boldsymbol{s}_0$ as one-dimensional vectors as well as $\boldsymbol{T}_t^{S_t}$, $\boldsymbol{R}_t^{S_t}$, and $\boldsymbol{Q}_t$ as 1×1-dimensional matrices.

In contrast, the observations $\boldsymbol{y}_t$ are two-dimensional. The measurement equation is given by

$$\boldsymbol{y}_t = \begin{pmatrix} \mathrm{RV}_t^{\mathrm{CLc1}} \\ \mathrm{OVX}_t^2 \end{pmatrix} = \boldsymbol{c}_t^{S_t} + \boldsymbol{Z}_t^{S_t}\boldsymbol{s}_t + \boldsymbol{e}_t \tag{27}$$

$$= \begin{pmatrix} c_{1,t}^{S_t} \\ c_{2,t} \end{pmatrix} + \begin{pmatrix} Z_{1,t}^{S_t} \\ Z_{2,t} \end{pmatrix} \boldsymbol{s}_t + \begin{pmatrix} e_{1,t} \\ e_{2,t} \end{pmatrix}, \tag{28}$$

with

$$\boldsymbol{e}_t = \begin{pmatrix} e_{1,t} \\ e_{2,t} \end{pmatrix} \sim \mathcal{N}_2\left(\boldsymbol{0}_{2\times 1}, \boldsymbol{H}\right), \tag{29}$$

and

$$\boldsymbol{H} = \begin{pmatrix} h_{11}^2 & 0 \\ 0 & h_{22}^2 \end{pmatrix}. \tag{30}$$

The first entry of the observation vector $\boldsymbol{y}_t$ is the realized variance of the Clc1 futures contract, and the second entry is the OVX^2 measure of the implied variance.

As assumed above, only the parameter π^{v,S_t} depends on the hidden Markov chain S_t in this simple model. Therefore, the Gaussian white noise $\boldsymbol{e}_t$ as well as the matrix $\boldsymbol{H}$ are independent of S_t, since π^{v,S_t} does not affect these quantities. The reason why $c_{2,t}$ and $Z_{2,t}$ are independent of S_t, is described below in (33) and (34). We have also assumed

that the white noise$\boldsymbol{e}_t$ is homoscedastic, i.e. that the matrix $\boldsymbol{H}$ is constant through time.

First, we cover the relationship between $v(t)$ (i.e.$\boldsymbol{s}_t$) and the realized variance $\mathrm{RV}_t^{\mathrm{CLc1}}$ of the Clc1 futures contract. We obtain from (16)

$$c_{1,t}^{S_t} = \tilde{\theta}^{S_t}\left(1 - \frac{1 - e^{-\tilde{\kappa}^{S_t}\tau}}{\tilde{\kappa}^{S_t}\tau}\right), \tag{31}$$

and

$$Z_{1,t}^{S_t} = \frac{1 - e^{-\tilde{\kappa}^{S_t}\tau}}{\tilde{\kappa}^{S_t}\tau}, \tag{32}$$

where $\tilde{\kappa}^{S_t} = \kappa - \sigma\pi^{v,S_t}$ and $\tilde{\theta}^{S_t} = \frac{\kappa\theta}{\kappa - \sigma\pi^{v,S_t}} = \frac{\kappa}{\tilde{\kappa}^{S_t}}\theta$. Note that (31) and (32) are calculated with respect to the physical measure $\mathbb{P}$; they are therefore *dependent* on the parameter π^{v,S_t} and the state of the hidden Markov chain S_t.

Second, we cover the relationship between v_t (i.e. $\boldsymbol{s}_t$) and the OVX^2. We obtain from (17)

$$c_{2,t} = \theta\left(1 - \frac{1 - e^{-\kappa\tau}}{\kappa\tau}\right), \tag{33}$$

and

$$Z_{2,t} = \frac{1 - e^{-\kappa\tau}}{\kappa\tau}. \tag{34}$$

Note that (33) and (34) are calculated with respect to the risk-neutral measure $\mathbb{Q}$; they are therefore *independent* of the parameter π^{v,S_t} and of the state of the hidden Markov chain S_t. Therefore, the relations

$$c_{2,t}^{S_t} = c_{2,t} \tag{35}$$

and

$$Z_{2,t}^{S_t} = Z_{2,t} \tag{36}$$

hold.

Estimation with the Kim filter. The Kim (1994) filter is an extension of the well-known Kalman filter for state-space models to *regime-switching* state-space models. (See also the book by Kim and Nelson (1999) for an in-depth description of this method.) A regime is a period of structural changes in the time series. Hamilton (1989) describes the shifts in regime as "episodes across which the dynamic behavior of the series is markedly different." Kim introduced the filter in the wake of the contributions of Hamilton (1989) and Lam (1990), and used it to study real GNP quarterly time-series figures from the U.S. post-war period from 1952 to 1984. In Lam (1990) and Kim (1994), one of the main goals of the filter is to detect "low-growth" and "high-growth" regimes in the data, and even assign numerical probabilities for being in a given regime.

Recall that the Kalman filter recursively derives a forecast of the usually unobserved state vector $\boldsymbol{s}_t$, based on information up to time t,

$$\boldsymbol{s}_{t|t} = \mathbb{E}\left[\boldsymbol{s}_t|\boldsymbol{\mathcal{F}}_t\right], \tag{37}$$

and the conditional variance-covariance matrix

$$\boldsymbol{\Sigma}_{t|t} = \mathrm{Var}\left(\boldsymbol{s}_t|\boldsymbol{\mathcal{F}}_t\right). \tag{38}$$

The aim of the Kim (1994) filter is to form a forecast of $\boldsymbol{s}_t$ not only conditioned on measurements $\boldsymbol{\mathcal{F}}_t$, but also conditioned on the hidden M-state Markov chain S_t.

Therefore, we define the conditional expectation of $\boldsymbol{s}_t$ given measurements $\boldsymbol{\mathcal{F}}_t$ up to time t, $S_{t-1} = i$, and $S_t = j$, as

$$\boldsymbol{s}_{t|t}^{(i,j)} := \mathbb{E}\left[\boldsymbol{s}_t|\boldsymbol{\mathcal{F}}_t, S_{t-1} = i, S_t = j\right]. \tag{39}$$

Furthermore, we define the conditional variance-covariance matrix of $\boldsymbol{s}_t$ as

$$\boldsymbol{\Sigma}_{t|t}^{(i,j)} := \mathrm{Var}\left(\boldsymbol{s}_t|\boldsymbol{\mathcal{F}}_t, S_{t-1} = i, S_t = j\right). \tag{40}$$

It should be noted that $\boldsymbol{s}_{t|t}^{(i,j)}$ from (39) as well as $\boldsymbol{\Sigma}_{t|t}^{(i,j)}$ from (40) would forecast M^2 different outcomes, corresponding to all possible combinations of i and j, at each time-point t. Therefore, it is necessary to apply some approximations to make this filter operable. The idea, according to Kim (1994), is to "collapse terms in the right way at

the right time". For our empirical study, we followed the steps of the algorithm described by Kim (1994), and implemented his filter in C++.

Like the Kalman filter, the Kim filter derives as a byproduct the conditional log-likelihood function

$$\ell\left(\boldsymbol{y}_1,\ldots,\boldsymbol{y}_T|\boldsymbol{\mathcal{F}}_0\right) := \ln\left(f\left(\boldsymbol{y}_1,\ldots,\boldsymbol{y}_T|\boldsymbol{\mathcal{F}}_0\right)\right) = \sum_{t=1}^{T} \ln\left(f_{\boldsymbol{y}_t|\boldsymbol{\mathcal{F}}_{t-1}}\left(\boldsymbol{y}_t|\boldsymbol{\mathcal{F}}_{t-1}\right)\right), \tag{41}$$

such that the unknown parameters of the state-space representation with regime-switching in (12) and (13), and in particular the transition probabilities from (14), can be estimated via maximum-likelihood estimation. The parameters to be estimated are listed in Table 5.

	1-State Model	**2-State Model**
$\mathbb{Q}$ mean-reversion speed	κ	κ
$\mathbb{Q}$ mean-reversion level	θ	θ
volatility	σ	σ
initial variance	v_0	v_0
market price of variance risk	π_v	π_v^0
	–	π_v^1
transition probability	–	$p_{0,1}$
	–	$p_{1,0}$

Table 5: Model Parameters to estimate

The $\mathbb{P}$-parameters $\tilde{\kappa}$ and $\tilde{\theta}$ for the 1-State Model, and $\tilde{\kappa}^0, \tilde{\kappa}^1$ and $\tilde{\theta}^0, \tilde{\theta}^1$ for the 2-State Model, are then directly obtained from equation (11).

We have the usual positivity restrictions for the first four parameters in Table 5, and also $p_{0,1}, p_{1,0} \in]0,1[$. Note also that the restrictions $\tilde{\kappa}^0, \tilde{\kappa}^1 > 0$ mean that we need to ensure $\pi_v^0, \pi_v^1 < \frac{\kappa}{\sigma}$ in the estimation. The two measurement error parameters $h_{0,0}, h_{1,1}$ are also included in our estimation procedure.

Last but not least, we point out that the Kim filter quantifies the probability of S_t being in state j at time t, given information $\boldsymbol{\mathcal{F}}_t$ up to time t. We will describe the results of our parameter estimation and the obtained probabilities in the next section.

4 Empirical Results

4.1 Parameter estimates

Our estimation is conducted on the data presented in Section 2, over the same period. The estimation relies on the Kim filter that we presented in Section 3.3. We contrast the outcomes of our Markov-switching model to those of a standard stochastic volatility model. The latter model corresponds to a model with a unique Markov state and is nested in our general case. It corresponds to a case where transition probabilities $p_{0,0}$ and $p_{1,1}$ are set to 1 and the initial state is set to 0 (which is the so-called normal state). The estimation of this model is conducted using a Kalman filter, even though we checked that the estimation with the Kim filter yielded similar parameter estimates. The parameter estimates of the two models are gathered in Table 6.

Several lessons can be drawn from the estimates in Table 6. First, the parameters relative to the variance dynamics under the risk-neutral probability – which are θ, κ, v_0, and σ – are roughly similar in both models. Except the initial value v_0, all these parameters are estimated to be significant (at the 5% and 1% levels) in both models. The first three parameters can interpreted in the context of unconditional mean $E[v_t|\mathcal{F}_0]$, whose expression is $v_0 e^{-\kappa t} + \theta(1 - e^{-\kappa t})$, as is standard for an Ornstein-Uhlenbeck process. Therefore, the expected variance starts from v_0 at initial date and converges to θ in the long-run with a convergence speed equal to κ. The initial value, v_0, is estimated to be very similar in both models. In the one-state model, it is equal to 6.53%, which corresponds to an annualized volatility of 25.56%, while in the two-state model, we respectively have 6.85% for the variance and 26.18% for the volatility. The long-run expected variance, θ, is 10.01% in the one-state model, which is slightly higher than the value of 7.15% in the two-state model. This means that the one-state model features an annualized volatility equal to 31.64%, while it is 26.73% in the two-state model. The mean reversion speed, κ, is quite higher in the two-state model that in the one-state, since it is equal to 11.6422 years^{-1} in the former case and 6.6167 years^{-1} in the latter. This represents quite strong mean reversion speeds, especially in the two-state model, as it implies that only 15 days are needed for the expectation $E[v_t|\mathcal{F}_0]$ to travel half the distance from initial value, v_0, to long-run value θ. The "half-life" amounts to 26 days in the case of the one-state model. Finally, the parameter σ, which is the volatility of the variance, can be interpreted

Parameters	Symbol	1-state model	2-state regime switching model
Speed of adjustment	κ	6.6167 (0.0935)	11.6422 (0.1782)
Long run value of variance	θ	0.1001 (0.0012)	0.0715 (0.0009)
Volatility	σ	0.8892 (0.0113)	0.9638 (0.0104)
Initial variance value	v_0	0.0653 (0.9990)	0.0685 (0.9994)
Market price of variance risk	$\pi_{v,0}$	1.6703 (0.2449)	−9.7268 (0.2544)
	$\pi_{v,1}$	–	11.2504 (0.1901)
Transition probabilities	$1-p_{0,0}$	0.0	0.0075 (0.0017)
	$1-p_{1,1}$	0.0	0.0284 (0.0067)
Std dev. of measurement errors	h_1	0.1055 (0.0013)	0.0061 (0.0001)
	h_2	0.0013 (0.0001)	0.0673 (0.0009)
Log-Likelihood	ℓ	11747.7	13650.2

Table 6: Estimates and standard errors (in brackets) of our model and the model without regime switches.

using the long-term unconditional variance of the variance process v_t, equal to $\frac{\sigma^2}{2\kappa}$, which amounts here to 5.97% in the one-state model and 3.99% in the two-state model. These values correspond to long-term variance volatility of 24.44% and 19.97%, respectively.

The standard deviation of measurement errors (see equations (27)–(30)) are quite different among the two models. Indeed, for the realized variance OVX^2, corresponding to parameter h_1, the error has a standard deviation of 10.55% in the one-state model, but only 0.61% in the two-state. Regarding implied variance corresponding to parameter h_2, this is the opposite: it amounts to 0.13% in the one-state model, but 6.73% in the two-state.

Obviously, both models differ drastically along the probabilities and the market price of variance risk. The probabilities we report in Table 6 are the probabilities to move from the crisis state to a normal state, $1 - p_{1,1}$, and the probability to transit from a normal state to a crisis state, $1 - p_{0,0}$. The former probability amounts to 2.84% (per day) and is significantly different from 0 (at the 5% and 1% levels). In other words, the expected length of a crisis is $(1 - p_{1,1})^{-1} \approx 35.2$ days. The probability to leave normal state for a crisis state is smaller and equals 0.75%, which implies that normal states feature an expected length of 134.0 days. The probability is also significantly different from 0 (at the 5% and 1% levels). Unsurprisingly, normal states are sizably more persistent than crisis states. Another view on this persistence is that these quantities imply that the unconditional probability to be in a normal state is $p_0 = 79.3\%$ and the one to be in a crisis state is the complement and equal to $p_1 = 20.8\%$. This is consistent with our interpretation of "normal" state for the more persistent and more frequent state 0 and of a crisis state for the other less frequent and less persistent state, 1.

The market price of variance risk is also drastically different between the models. The price is positive and equal to 1.67 (and significantly different from 0) in the one-factor model. In the two-factor model, the price is still positive but much higher to 11.25 in the crisis state. In the normal state, the price is negative and equal to -9.73. Both prices are significantly different from 0. This pleads in favor of the separation between the two states, which cover episodes in which the market price of variance risk is dramatically different. Separating the two states enables us to observe that not only the price of variance risk differs among states, but its sign is even different: the variance risk turns out to have a positive price in crisis states.

Finally, we can conclude the comparison between the two models by comparing their log-likelihood. Since the one-state is nested within the two-state model, we can conduct a likelihood-ratio test, consisting in computing twice the difference between log-likelihoods. Formally, the test statistics is defined as:

$$t_\ell = 2(\ell_{2f} - \ell_{1f}), \tag{42}$$

where ℓ_{1f} and ℓ_{2f} are the log-likelihoods of the one- and two-state models respectively. The null hypothesis is that the "true" model is the one-state model, which is the smallest model of the two. A large value for the test statistics means that the rejection of the

null hypothesis. The statistics follows asymptotically a χ^2 distribution with a number of degrees of freedom equal to the difference of dimensionality between the two models, equal to 3 here. Indeed, the two-state model additionally features, compared to the one-state, two parameters for probability and one for the market price of risk. In our case, we have $t_\ell \approx 3804.9$, which is far greater than the value of 16.3, which is the threshold at the 0.1% level. We can thus be confident that the two-state provides a significantly better fit to the data than the one-state model.

4.2 Probabilities

4.2.1 Description

One of the model's outcomes is the computation of the times series of filtered probabilities. Since our model only features two states, each probability is the complement of the other one. We report in Figure 4 the probabilities to be in the crisis state over our sample, as computed by our model estimated on the OVX data. We also report the same probabilities, but computed for US GDP data. We also report in shaded gray the contraction periods of the NBER.[3] We can see that both probabilities are positively correlated – the formal correlation amounting to 34%. This is especially visible in 2008-2009 and in early 2021. The high probabilities values for GDP are also consistent with the NBER timing of contractions. However, a number of episodes of high probabilities for OVX crisis state are not reflected in GDP data (see 2012 or 2016 for instance).

The OVX crisis probability data are highly concentrated around two poles, 0 and 1. More precisely, approximately 75% of probabilities are smaller than 10%, while almost 20% of them are greater than 90%. Around 5% of data points are between 10% and 90%. Furthermore, we can check that the crisis probability also connects to VRP and to the results of Table 5. We report in Table 7 the conditional statistics regarding episodes of high and low probabilities. We consider a threshold of 0.5 for distinguishing high from low probabilities. A date t will hence be considered as a crisis if the filtered probability as that state is greater than 0.5. Conversely, the date will be considered as a normal state. We also report the correlations of filtered probabilities with the same quantities as in Table 5.

[3] See `https://www.nber.org/research/data/us-business-cycle-expansions-and-contractions`.

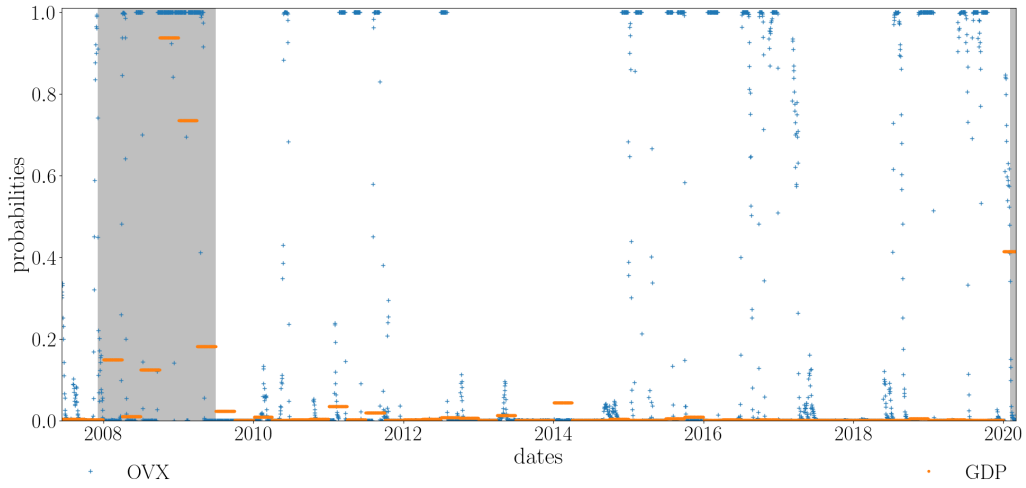

Figure 4: Time-series probabilities for OVX and GDP data.

Table 7 confirms the intuitions stated in Section 2. The crisis state is characterized by positive VRP, while the normal state features negative VRP. The two states therefore enable to distinguish between episodes of positive VRP from negative ones. This is also reflected in the high correlation (around 60%) between the crisis probabilities and VRP. Furthermore, crisis states are also characterized by high realized and implied volatilities, as well as low and negative 21-day CLc2 returns. CLc1 prices also tend to be smaller in crisis states than in normal ones. One-day CLc1 returns are pretty similar in crisis and normal states. Comparing to Table 5, we can observe that the overall pattern of conditional moments is pretty similar: conditioning on the sign of the VRP yields overall similar results to when conditioning on the crisis probability being above or below 0.5.

4.2.2 OVX probabilities and conditional CAPM

In this section, we investigate to which extent using the uncovered OVX probabilities can improve the CAPM on variance risk premium. More precisely, we test in the cross-section to which extent the variance risk premium can be explained by the 21-day (log) return on CLc contracts. The return and the variance risk premium therefore cover exactly the same time-span. The log return we consider is the log-return associated to buying a CLc2 contract at some date and reselling it 21 working days later as a CLc1 contract. We

[4]The 21-day CLc2 log-return is defined as $\ln(\text{CLc1}_t/\text{CLc2}_{t-20})$, where CLc1_t is the date-t price of the CLc1 contract and $\text{CLc2}_{t-20}$the date $t-20$ price of the CLc2 contract.

	Unconditional	Crisis prob.s ≥ 0.5	Crisis prob.s < 0.5	Correlations with Crisis prob.s(%)
Number of observations	3185	715	2470	–
$\text{VRP}_{t-20,t}$ (%)	-1.04 (10.58)	10.14 (16.48)	-4.28 (4.38)	59.17
Realized variance $\text{RV}^{\text{CLc1}}_{t,t+20}$ (%)	13.68 (18.33)	25.74 (27.78)	10.19 (12.48)	36.61
Realized variance $\text{RV}^{\text{CLc1}}_{t-20,t}$ (%)	13.68 (18.33)	33.55 (29.31)	7.93 (6.12)	60.60
OVX2 (%) (OVX^2_t)	14.75 (12.49)	26.26 (18.80)	11.41 (7.04)	51.55
CLc1 price $F(t, T_1)$ (USD)	74.12 (23.04)	61.96 (23.50)	77.65 (21.68)	-28.44
1-day CLc1 log-return (%)	-0.01 (2.24)	-0.06 (3.40)	0.01 (1.77)	-0.93
21-day CLc2 log-return (%)[4]	-0.86 (10.03)	-5.73 (13.61)	0.55 (8.20)	-26.95

Table 7: Conditional statistics regarding episodes of high and low probabilities to be in a crisis state. In the last column, we also report the correlations of the crisis probabilities with various quantities.

denote this return as $r_{21,t}$, which we have called the 21-day CLc2 log-return in Footnote 4. It is defined as: $r_{21,t} = \ln(\text{CLc1}_t/\text{CLc1}_{t-20})$. The CAPM regressions we run is:

$$\text{VRPL}_{t-20,t} = \alpha + \beta r_{21,t} + \varepsilon_t, \tag{43}$$

where $(\varepsilon_t)_{t\geq 0}$ are error terms. The results are gathered in Table 8. As can be seen, the regression has a very low explanatory power and the R^2 coefficient remains quite low: around 10%.

We now investigate to how much knowing probabilities, and hence latent states, improves the predictive power of the cross-sectional regression. We thus consider a conditional CAPM. We first allow the intercept coefficient α to depend on the state. To

determine the state, we follow Table 7. We use the cut-off value of 50% and condition on whether the crisis probability, denoted by p_t, is greater or smaller than 50%.[5] We thus run the two following regression:

$$\text{VRPL}_{t-20,t} = \alpha_u 1_{p_t \geq 50\%} + \alpha_d 1_{p_t < 50\%} + \beta r_{21,t} + \varepsilon_t. \tag{44}$$

The results of the regression are gathered in Table 8. All coefficients are still significant and the R^2 for both regressions increases by a large amounts. It reaches 42.2% (up from 10.4%) for the log VRP expression (2). This increase in the explanatory power can be explained by the change of sign of the intercept coefficient α that remain negative in normal times (as in the baseline regression) but turns out to be positive in crisis times (state 1).

We finally further refine the regression and allow for β to be state-dependent. We run the following regressions:

$$\text{VRPL}_{t-20,t} = \alpha_u 1_{p_t \geq 50\%} + \alpha_d 1_{p_t < 50\%} + \beta_u r_{21,t} 1_{p_t \geq 50\%} + \beta_d r_{21,t} 1_{p_t < 50\%} + \varepsilon_{2,t}. \tag{45}$$

Table 8 gathers the regression results. The regression coefficients βs keep the same signs as in regression (44), but with different magnitudes. In particular, we have $0 > \beta_u > -1 > \beta_d$. However, the increase in the R^2 is modest when adding state-dependent βs, highlighting that most of the benefit stems from the state-dependent intercept.

5 Trading Realized vs Implied Variance

We now focus our attention on trading strategies and the use of our "regime-probabilities" (see Figure 4) as trading signals.

So far, we have adopted a "variance swap" point of view in order to study the variance risk premium. We compared the OVX_t^2 at time a given t to the future realized variance $\text{RV}_{t,t+20}^{\text{CLc1}}$ of the beginning 21-day trading period. Now we shift it to an "$\mathcal{F}_t$" point of view in order to use all the available information at time t, i.e. we use the OVX_t^2 and

[5] The results are not sensitive to a precise value of the cut-off and given the distribution of probabilities, any value in the range $[5\%; 95\%]$ yields very similar results.

	Regression (43)	Regression (44)	Regression (45)
α	-0.314 (0.009)	–	–
α_u	–	0.262 (0.016)	0.280 (0.016)
α_d	–	-0.472 (0.008)	-0.471 (0.008)
β	-1.720 (0.088)	-0.922 (0.073)	–
β_u	–	–	-0.602 (0.110)
β_d	–	–	-1.177 (0.098)
R^2	10.70%	42.18%	42.46%

Table 8: Results of the regressions (43)–(45). Point estimates and standard errors in brackets.

the historic realized variance $\mathrm{RV}^{\mathrm{CLc1}}_{t-20,t}$. We re-estimate our model parameters for this shifted time series $(\mathrm{RV}^{\mathrm{CLc1}}_{t-20,t}, \mathrm{OVX}^2_t)_{t=1,\ldots,3204}$, with t_1 denoting the date 11/06/2007, on which CLc1 closed at USD 65.97, and t_{3204} denoting the date 02/03/2020, on which CLc1 closed at USD 46.75.

Interestingly, the log-likelihood score of the estimation increases from 13650.2 to 14520.7. The model parameters only change very little; the increase in the ll-score seems to come from both h_1 and h_2 now being smaller: before the values were $h_1^{VS} = 0.0061, h_2^{VS} = 0.0673$ (see Subsection 4.1 for the previous parameter estimates); the new values are $h_1^{\mathcal{F}_t} = 0.0022, h_2^{\mathcal{F}_t} = 0.0535$. So when the model is estimated using data available at time t, then it seems to fit slightly better.

There are various ways of trading volatility and variance on financial markets. One is via variance swaps, as discussed previously. Another well-known strategy is called "gamma-hedging" or "gamma scalping". If a trader believes that future realized volatility will be higher than the currently observed implied volatility, the trader buys a call option and then delta-neutralizes it by going short the underlying share or futures contract. As the market moves, the trader re-balances the hedge to stay delta-neutral, for example on a daily basis. This leads in effect to a profitable "buy low, sell high" policy in the underlying, and the more volatile the market is, the more profitable this strategy is likely to be. In case the trader anticipates lower future realized volatility, he can sell the

option and go through the opposite hedging strategy. If the market moves only little, this strategy will be profitable. A more sophisticated version of gamma scalping consists in buying or selling several options with different strikes in order to account for the volatility smile, and then delta-hedging this option portfolio.

In the remainder of this section, we analyze strategies to directly trade the realized variance $\mathrm{RV}^{\mathrm{CLc1}}_{t,t-20}$ against the OVX^2_t, i.e. to trade their difference or "spread". We examine five strategies:

(i). always going long this difference, i.e. trading $\Delta_t := \mathrm{RV}^{\mathrm{CLc1}}_{t-20,t} - \mathrm{OVX}^2_t$ on each day in our time series;

(ii). always going short, i.e. trading $-\Delta_t = \mathrm{OVX}^2_t - \mathrm{RV}^{\mathrm{CLc1}}_{t-20,t}$ on each day;

(iii). using the probabilities obtained via the Kim-filter as a trading signal: given a threshold $\tau \in [0,1]$, we go long Δ_t if $\mathbb{P}(S_t = 1) \geq \tau$, and short otherwise;

(iv). use a "naive" signal based on the previous day's sign of Δ_t;

(v). use both of these signals "jointly" and only trade if they point in the same direction.

The "probabilities-based" and "naive" trading strategy are illustrated in Table 9. The strategies were initialized with the model being in the "normal" state $S_t = 0$, and therefore going short, and for a threshold value $\tau = 0.5$.

Table 10 summarizes the five strategies by showing the numbers of negative and positive trades, the overall P & L, the average P & L per trade, and the standard deviation of the daily profit or loss.

We can see that the "always long" strategy leads to an overall loss of -35.77, with 2492 negative (loss-making) trades and 712 positive (profitable) trades. The "always short" strategy is obviously the opposite and leads to an overall profit of 35.77, with 712 negative and 2492 positive trades. This is in agreement with the VRP being negative in the majority of cases, although we cannot directly compare these numbers to those reported in Table because we have switched from $\mathrm{RV}^{\mathrm{CLc1}}_{t,t+20}$ to $\mathrm{RV}^{\mathrm{CLc1}}_{t-20,t}$.

The next three strategies perform much better. The "probabilities" strategy leads to a profit of 160.56, with 403 negative and 2801 positive trades, and an average profit of 0.0501 with standard deviation 0.0851. The "naive" strategy leads to a profit of 176.85, with 170 negative and 3034 positive trades, and an average profit of 0.0552 with standard

Time	$\mathbf{RV}^{\mathbf{CLc1}}_{t,t-20}$	$\mathbf{OVX}^{\mathbf{2}}_{t}$	p_t (%)	prob. based	P&L (daily)	P&L (cum.)	naive	P&L (daily)	P&L (cum.)
1	0.0800	0.0675	33.48	-1	-0.0124	-0.0124	1	-0.0124	-0.0124
2	0.0812	0.0666	33.12	-1	-0.0146	-0.0271	1	0.0146	0.0022
3	0.0828	0.0680	33.23	-1	-0.0148	-0.0419	1	0.0148	0.0170
4	0.0857	0.0694	35.50	-1	-0.0163	-0.0581	1	0.0163	0.0333
5	0.0836	0.0697	32.08	-1	-0.0138	-0.0720	1	0.0138	0.0471
⋮	⋮	⋮	⋮	⋮	⋮	⋮	⋮	⋮	⋮
3199	0.0738	0.1563	0.00	-1	0.0824	159.94	-1	0.0824	176.23
3200	0.0765	0.1806	0.00	-1	0.1041	160.04	-1	0.1041	176.33
3201	0.0783	0.1884	0.00	-1	0.1101	160.15	-1	0.1101	176.44
3202	0.0869	0.2442	0.00	-1	0.1573	160.31	-1	0.1573	176.60
3203	0.1094	0.2627	0.00	-1	0.1532	160.46	-1	0.1532	176.75
3204	0.1368	0.2336	0.00	-1	0.0968	**160.56**	-1	0.0968	**176.85**

Table 9: Probabilities-based vs Naive Trading Strategy

deviation 0.0819. Finally, using both signals together leads to a profit of 168.70, with 99 negative and 2730 positive trades, and an average profit of 0.0527 with standard deviation 0.0814.

On closer inspection, the naive strategy outperforms the probabilities-based strategy because it reacts immediately to a change in sign of the spread Δ_t, whereas the probability-based strategy is based on a filtering procedure and reacts less quickly. However, in an actual trading implementation, this could lead to less frequent reversals of

strategy	always long	always short	p.b.	naive	joint
negative	2492	712	403	170	99
positive	712	2492	2801	3034	2730
profit	-35.77	35.77	160.56	176.85	168.70
average	-0.0112	0.0112	0.0501	0.0552	0.0527
std. dev.	0.0981	0.0981	0.0851	0.0819	0.0814

Table 10: Summary of Trading Strategies

direction and therefore reduced trading costs. Also, using both signals together reduces the number of negative trades from 170 to 99, and also slightly the standard deviation.

We also point out that the probabilities-based strategy is rather robust with regards to the probability threshold τ. Table 11 shows the P & L of this strategy as a function of the probability threshold used.

0.0	0.1	0.3	0.4	0.5	0.6	0.7	0.9	1.0
-35.77	156.99	159.31	159.78	160.56	160.74	161.77	162.88	35.77

Table 11: Threshold for Trading Signal

6 Conclusion

In this paper, we have presented a regime-switching volatility model for the oil market. We introduce regime switches while preserving tractability. Indeed, only the market price of volatility risk is affected by the changes of regimes, while the risk-neutral dynamics of the model remains the same in all regimes. The risk-neutral model features Samuelson volatility effect and stochastic volatility. This tractability allows us to estimate the model on OVX and futures data using a Kim filter. One result of the estimation is that the model enables us to distinguish two regimes: on the one hand a crisis state featuring positive variance risk premium, high realized volatility and high implied volatility and on the other hand a normal state with a negative variance risk premium, low realized volatility and low implied volatility.

Another lesson from the model estimation is that the crisis probabilities inferred from the oil market are correlated to the crisis probabilities inferred from GDP data. In particular, in both cases, the 2008 crisis and the beginning of the Covid crisis are visible. However, the oil data probabilities imply more "frequent" crisis than GDP data. A possible route for future research would be to confront the estimated probabilities on the oil market to those estimated on the stock market. This could enable us to distinguish financial shocks that have affected the two markets from market-specific shocks.

References

Gurdip Bakshi and Dilip Madan. Spanning and derivative-security valuation. *Journal of Financial Economics*, 55(2):205–238, 2000.

Fisher Black and Myron Scholes. The pricing of options and corporate liabilities. *Journal of Political Economy*, 81:637–654, May-June 1973.

Peter Carr and Liuren Wu. Variance risk premiums. *Review of Financial Studies*, 22(3): 1311–1341, 2009.

Jaime Casassus and Pierre Collin-Dufresne. Stochastic convenience yield implied from commodity futures and interest rates. *Journal of Finance*, 60(5):2283–2331, October 2005.

Carl Chiarella, Boda Kang, Christina Sklibosios Nikitopoulos, and Thuy-Duong Tô. Humps in the volatility structure of the crude oil futures market: New evidence. *Energy Economics*, 40:989–1000, 2013.

Iain J. Clark. *Commodity Option Pricing: A Practitioner's Guide*. Wiley Finance. Wiley, 2014.

Les Clewlow and Chris Strickland. Valuing energy options in a one factor model fitted to forward prices. Working Paper, 30 pages, April 1999.

J. C. Cox, J. E. Ingersoll, and S. A. Ross. A theory of the term structure of interest rates. *Econometrica*, 53:385–408, 1985.

James S. Doran and Ehud I. Ronn. Computing the market price of volatility risk in the energy commodity markets. *Journal of Banking and Finance*, 32:2541–2552, 2008.

Robert J. Elliott, Leunglung Chan, and Tak Kuen Siu. Option pricing and Esscher transform under regime switching. *Annals of Finance*, 1:423–432, 2005.

Viviana Fanelli. *Financial Modelling in Commodity Markets*. Financial Mathematics Series. Chapman and Hall/CRC, first edition, 2019.

James D. Hamilton. A new approach to the economic analysis of nonstationary time series and the business cycle. *Econometrica*, 57(2):357–384, March 1989.

James D. Hamilton and Jing Cynthia Wu. Identification and estimation of Gaussian affine term structure models. *Journal of Econometrics*, 91(168):315–331, 2012.

Steven Heston. A closed-form solution for options with stochastic volatility with applications to bond and currency options. *Review of Financial Studies*, 6(2):327–343, 1993.

Chang-Jin Kim. Dynamic linear models with Markov-switching. *Journal of Econometrics*, 60(1–2):1–22, January/February 1994.

Chang-Jin Kim and Charles R. Nelson. *State-Space Models with Regime Switching: Classical and Gibbs-Sampling Approaches with Applications*. MIT Press, 1999.

Pok-Sang Lam. The Hamilton model with a general autoregressive component: Estimation and comparison with other models of economic time series. *Journal of Monetary Economics*, 26(3):409–432, December 1990.

Robert C. Merton. Theory of rational option pricing. *Bell Journal of Economics and Management Science*, 4(1):141–183, 1973.

Andrew Papanicolaou and Ronnie Sircar. A regime-switching Heston model for VIX and S&P 500 implied volatilities. *Quantitative Finance*, 14(10):1811–1827, 2014.

Andrea Roncoroni, Gianluca Fusai, and Mark Cummins. *Handbook of Multi-Commodity Markets and Products: Structuring, Trading and Risk Management*. Wiley Finance Series. Wiley, 2015.

Paul A. Samuelson. Proof that properly anticipated prices fluctuate randomly. *Industrial Management Review*, 6(2):41–49, Spring 1965.

Lorenz Schneider and Bertrand Tavin. From the Samuelson volatility effect to a Samuelson correlation effect: An analysis of crude oil calendar spread options. *Journal of Banking and Finance*, 95:185–202, October 2018.

Lorenz Schneider and Bertrand Tavin. Seasonal volatility in agricultural markets: Modelling and empirical investigations. *Annals of Operations Research*, 2021. To appear.

Anders B. Trolle and Eduardo S. Schwartz. Unspanned stochastic volatility and the pricing of commodity derivatives. *Review of Financial Studies*, 22(11):4423–4461, 2009.

Anders B. Trolle and Eduardo S. Schwartz. Variance risk premia in energy commodities. *Journal of Derivatives*, 17(3):15–32, Spring 2010.

Ruey S. Tsay. *Analysis of Financial Time Series*. Series in Probability and Statistics. Wiley, third edition, 2010.

Appendix

A The VIX and the stock market

We present here the results of our methodology applied to the stock market, instead of the oil market. More precisely, we use the S&P500 (henceforth, SPX) and the associated VIX volatility index.

A.1 The data

We start with plotting in Figure 5 the realized variance time series for the SPX and compare it to the two VIX^2 time series. This is the parallel of Figure 1 that was plotted for Clc1 and OVX. The two main messages that held for the oil market are still valid here. First, long periods of low variance – either implied or realized – are interrupted by short periods of very high variance. Second, the implied volatility is usually higher than the realized variance except in periods of high variance. The main difference compared to the Figure 1 is that besides the spike of 2008, the variance data for stocks present fewer and lower spikes.

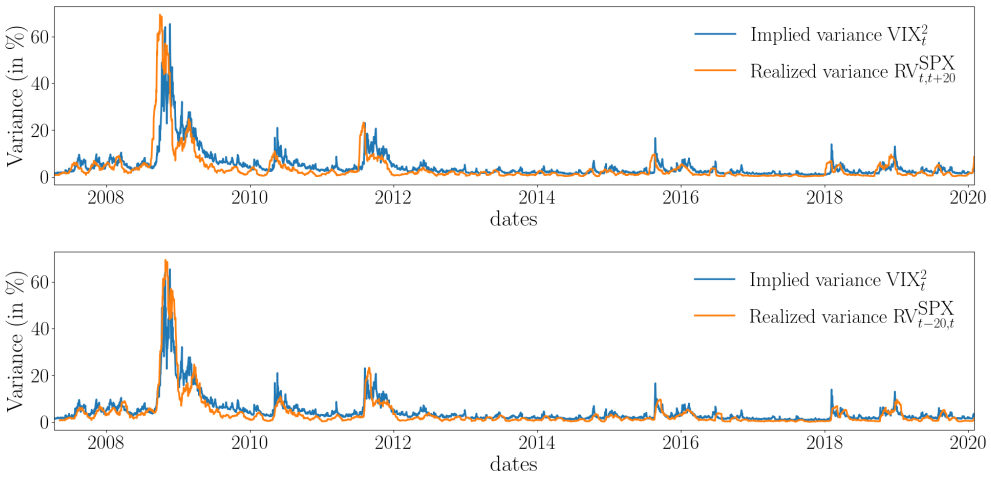

Figure 5: OVX^2 and CLc1 realized variance, from 10 May 2007 to 31 January 2020.

To illustrate the last point, we report in Table 12 some descriptive statistics regarding realized and implied variances – as we did in Table 3 for OVX. This confirms what was

visible on Figure 5, as well as the comparison with OVX data.

	Implied variance (VIX_t^2)	Realized variance ($\text{RV}_{t,t+20}^{\text{SPX}}$)	Realized variance ($\text{RV}_{t-20,t}^{\text{SPX}}$)
Mean	4.59%	3.68%	3.69%
Standard Error	5.91%	7.48%	7.48%
Minimum	0.84% (on 3 Nov 2017)	0.11% (on 13 Nov 2017)	0.11% (on 11 Oct 2017)
Q25	1.82%	0.81%	0.82%
Median	2.78%	1.66%	1.66%
Q75	4.93%	3.60%	3.61%
Maximum	65.38% (on 20 Nov 2008)	69.39% (on 30 Sep 2008)	69.39% (on 28 Oct 2008)
Correlation with VIX_t^2	100.0%	74.1%	90.4%

Table 12: Realized vs Implied variance, from 10 May 2007 to 31 January 2020.

As we did for OVX, we define the variance risk premia as follows:

$$\text{VRP}_{t,t+20}^{\text{SPX}} = \text{RV}_{t,t+20}^{\text{SPX}} - \text{VIX}_t^2,$$
$$\text{VRPL}_{t,t+20}^{\text{SPX}} = \ln(\text{RV}_{t,t+20}^{\text{SPX}}/\text{VIX}_t^2),$$

where we use the SPX superscript to highlight that we focus on SPX and VIX. In Figure 5, we observed that the realized variance was below the implied one, except for some episodes. It is thus expected that, as for the OVX, the variance risk premium is most of the time and on average negative and that episodes of positive VRP are exceptional and an indicator of special times. As we did in Table 5, we report in Table 13 several conditional statistics so as to better contrast the episodes of positive volatility to those of negative volatility.

Similarly to what we found in the OVX case, the episodes of positive variance risk premium corresponds to a high implied and realized volatility, as well as negative 21-day returns. These episodes can thus be thought of as crisis as was the case for the oil market.

	Unconditional	Positive VRP	Negative VRP
Number of observations	3185	520	2665
$\mathrm{VRP}^{\mathrm{SPX}}_{t-20,t}$ (%)	-0.93 (5.06)	4.81 (9.50)	-2.05 (2.30)
Realized variance $\mathrm{RV}^{\mathrm{SPX}}_{t,t+20}$ (%)	3.70 (7.50)	8.84 (15.46)	2.70 (3.82)
Realized variance $\mathrm{RV}^{\mathrm{SPX}}_{t-20,t}$ (%)	3.70 (7.50)	9.93 (14.60)	2.48 (4.09)
VIX2 (%) (VIX^2_t)	4.63 (5.94)	8.62 (10.45)	3.85 (4.14)
SPX index (points)	1811.02 (633.65)	1800.37 (635.04)	1813.10 (633.48)
1-day SPX log-return (%)	0.02 (1.23)	-0.03 (2.11)	0.04 (0.97)
21-day SPX log-return (%)	0.48 (4.57)	-4.76 (5.73)	1.51 (3.49)

Table 13: Conditional statistics regarding episodes of positive and negative VRP.

A.2 Model and estimation

We thus also consider a regime-switching model that we estimate based on VIX data. The estimation procedure is the same as the one described in Section 3.3 and relies on the Kim filter. The estimated parameters of the one- and two-factor models are gathered in Table 14.

As in the OVX case, most estimates are significant – with the sole exception of the initial variance value. As in the OVX case, the one- and two-factor models mostly differ along the market price of variance risk. It is positive in the one-factor model and its sign depends on the state in the two-factor model. This is similar to what was observed in the parameters estimates on OVX data. Finally, comparing the two models using the likelihood-ratio test of equation (42) yields a statistic $t_\ell^{\mathrm{VIX}} = 1167.3$, which is far larger than the threshold of 16.3 at the 0.1% level. The two-factor model therefore provides a better fit to the data than the one-factor model.

Parameters	Symbol	1-state model	2-state regime switching model
Speed of adjustment	κ^{SPX}	(0.1592)	4.9337 (0.1670)
Long run value of variance	θ^{SPX}	0.0100 (0.0004)	0.0176 (0.0006)
Volatility	σ^{SPX}	0.4137 (0.0053)	0.5468 (0.0096)
Initial variance value	v_0^{SPX}	0.0150 (0.9763)	0.0119 (0.8997)
Market price of variance risk	$\pi_{v,0}^{\text{SPX}}$	8.0000 (0.5271)	−19.9974 (0.5792)
	$\pi_{v,1}^{\text{SPX}}$	–	8.0000 (0.4053)
Transition probabilities	$1-p_{0,0}^{\text{SPX}}$	0.0	0.0100 (0.0026)
	$1-p_{1,1}^{\text{SPX}}$	0.0	0.0491 (0.0128)
Std dev. of measurement errors	h_1^{SPX}	0.0003 (0.0000)	0.0006 (0.0000)
	h_2^{SPX}	0.0480 (0.0006)	0.0409 (0.0005)
Log-Likelihood	ℓ^{SPX}	19236.9	19820.5

Table 14: Estimates and standard errors (in brackets) of our model and the model without regime switches.

A.3 Results

We start with plotting in Figure 6 the probability to be in the "crisis" state according to the VIX model. As in Figure 4, we also report for the sake of comparison the probabilities computed using GDP data and the contraction periods of the NBER. There is still a positive correlation between the VIX and the GDP probabilities that amount to 25.8%. There is also a positive correlation of 41.0% between the VIX and OVX probabilities.

We also compute some descriptive statistics conditional on the state – as done in Table 5. These computations are reported in Table 15. The pattern is similar to the one found in the case of OVX. The crisis state corresponds to high realized and implied

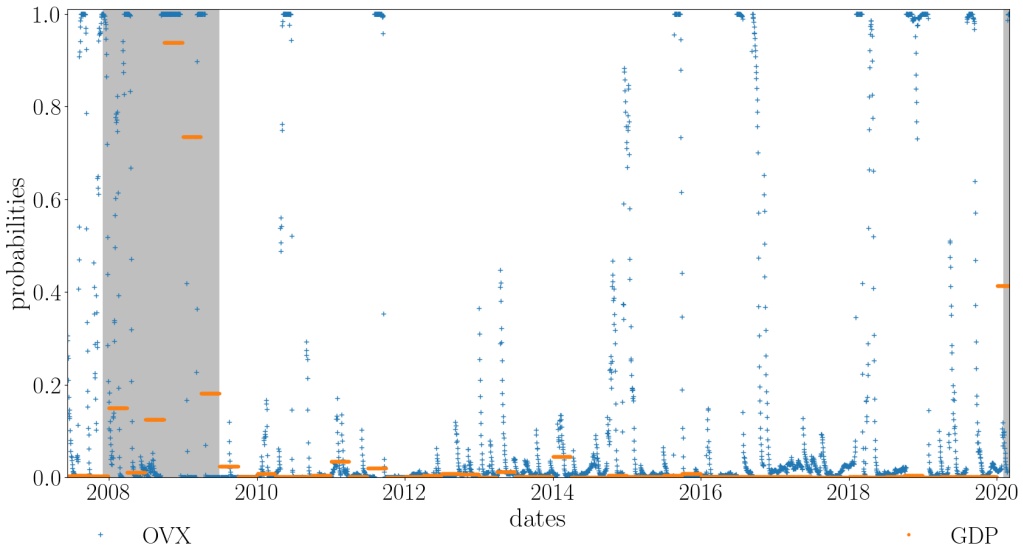

Figure 6: Time-series probabilities for VIX and GDP data.

volatility, as well as negative one-month returns.

Finally, we also investigate the conditional CAPM to assess probabilities how much knowing probabilities help improve the predictive power of the cross-sectional regression. We start with our benchmark, the unconditional CAPM:

$$\text{VRPL}_t^{\text{SPX}} = \alpha^{\text{SPX}} + \beta^{\text{SPX}} r_{21,t}^{\text{SPX}} + \varepsilon_t^{\text{SPX}}, \tag{46}$$

where $(\varepsilon_t^{\text{SPX}})_{t\geq 0}$ are error terms and $r_{21,t} = \ln(SPX_t/SPX_{t-21})$ is the 21-day log-return on the SPX. The two conditional regressions that we consider are:

$$\text{VRPL}_t^{\text{SPX}} = \alpha_u^{\text{SPX}} 1_{p_t^{\text{SPX}} \geq 50\%} + \alpha_d^{\text{SPX}} 1_{p_t^{\text{SPX}} < 50\%} + \beta^{\text{SPX}} r_{21,t}^{\text{SPX}} + \varepsilon_t^{\text{SPX}}, \tag{47}$$

and

$$\begin{aligned} \text{VRPL}_t^{\text{SPX}} = {} & \alpha_u^{\text{SPX}} 1_{p_t^{\text{SPX}} \geq 50\%} + \alpha_d^{\text{SPX}} 1_{p_t^{\text{SPX}} < 50\%} \\ & + \beta_u^{\text{SPX}} r_{21,t}^{\text{SPX}} 1_{p_t^{\text{SPX}} \geq 50\%} + \beta_d^{\text{SPX}} r_{21,t}^{\text{SPX}} 1_{p_t^{\text{SPX}} < 50\%} + \varepsilon_t^{\text{SPX}}. \end{aligned} \tag{48}$$

The results of all these regressions are gathered in Table 16. As can be seen, the coefficients of all regressions are significant at the 1% level and allowing for state-dependent coefficient boosts the R^2 coefficient by a large extent.

	Unconditional	Crisis prob.s ≥ 0.5	Crisis prob.s < 0.5	Correlations with Crisis prob.s(%)
Number of observations	3185	502	2683	–
$\mathrm{VRP}^{\mathrm{SPX}}_{t-20,t}$ (%)	-0.93 (5.06)	3.99 (10.30)	-1.85 (2.27)	44.61
$\mathrm{RV}^{\mathrm{SPX}}_{t,t+20}$ (%)	3.70 (7.50)	9.85 (15.57)	2.55 (3.63)	36.26
$\mathrm{RV}^{\mathrm{SPX}}_{t-20,t}$ (%)	3.70 (7.50)	12.07 (15.44)	2.13 (2.60)	50.01
VIX2 (%) (VIX^2_t)	4.63 (5.94)	10.19 (11.24)	3.59 (3.37)	41.73
SPX index (points)	1811.02 (633.65)	1776.16 (710.12)	1817.54 (618.22)	-1.43
1-day SPX log-return (%)	0.02 (1.23)	-0.07 (2.25)	0.04 (0.92)	-2.81
21-day SPX log-return (%)	0.48 (4.57)	-3.18 (7.10)	1.17 (3.53)	-37.59

Table 15: Conditional statistics regarding episodes of high and low probabilities to be in a crisis state. In the last column, we also report the correlations of the crisis probabilities with various quantities.

	Regression (46)	Regression (47)	Regression (48)
α^{SPX}	-0.550 (0.010)	–	–
α^{SPX}_u	–	0.171 (0.022)	0.195 (0.023)
α^{SPX}_d	–	-0.699 (0.009)	-0.693 (0.010)
β^{SPX}	-9.441 (0.217)	-7.039 (0.197)	–
β^{SPX}_u	–	–	-6.278 (0.300)
β^{SPX}_d	–	–	-7.614 (0.260)
R^2	37.18%	54.80%	54.96%

Table 16: Results of the regressions (46)–(48). Point estimates and standard errors in brackets.